JACS
JOURNAL OF THE AMERICAN CHEMICAL SOCIETY

Article

pubs.acs.org/JACS

Calculated pK_a Variations Expose Dynamic Allosteric Communication Networks

Eric J. M. Lang,[†,∥] Logan C. Heyes,[†,∥] Geoffrey B. Jameson,[§] and Emily J. Parker*[,‡]

[†]Biomolecular Interaction Centre and Department of Chemistry, and [‡]Maurice Wilkins Centre, Biomolecular Interaction Centre and Department of Chemistry, University of Canterbury, PO Box 4800, Christchurch 8140, New Zealand

[§]Institute of Fundamental Sciences, Massey University, PO Box 11-222, Palmerston North 4422, New Zealand

Supporting Information

ABSTRACT: Allosteric regulation of protein function, the process by which binding of an effector molecule provokes a functional response from a distal site, is critical for metabolic pathways. Yet, the way the allosteric signal is communicated remains elusive, especially in dynamic, entropically driven regulation mechanisms for which no major conformational changes are observed. To identify these dynamic allosteric communication networks, we have developed an approach that monitors the pK_a variations of ionizable residues over the course of molecular dynamics simulations performed in the presence and absence of an allosteric regulator. As the pK_a of ionizable residues depends on their environment, it represents a simple metric to monitor changes in several complex factors induced by binding an allosteric effector. These factors include Coulombic interactions, hydrogen bonding, and solvation, as well as backbone motions and side chain fluctuations. The predictions that can be made with this method concerning the roles of ionizable residues for allosteric communication can then be easily tested experimentally by changing the working pH of the protein or performing single point mutations. To demonstrate the method's validity, we have applied this approach to the subtle dynamic regulation mechanism observed for *Neisseria meningitidis* 3-deoxy-D-*arabino*-heptulosonate 7-phosphate synthase, the first enzyme of aromatic biosynthesis. We were able to identify key communication pathways linking the allosteric binding site to the active site of the enzyme and to validate these findings experimentally by reestablishing the catalytic activity of allosterically inhibited enzyme via modulation of the working pH, without compromising the binding affinity of the allosteric regulator.

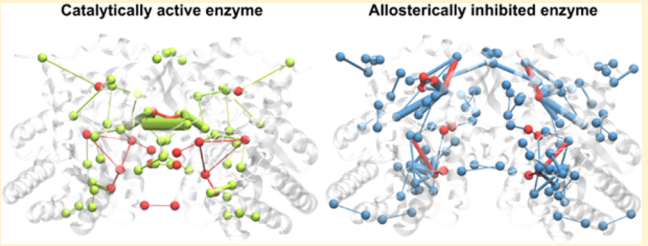

INTRODUCTION

Allosteric regulation of protein function is critical to cellular metabolic control. Allostery is the process by which the binding of a ligand provides a functional response at a distant site, and is essential for cell signaling events and sophisticated metabolic control through the regulation of enzymatic catalysis. Traditional models of allostery described the allosteric response as being mediated by large conformational changes that directly affect activity.[1,2] However, using the formalism of statistical mechanics, Cooper and Dryden[3] proposed that allostery could exist even in the absence of conformational changes via a purely dynamic, entropically driven, mechanism. As noted recently,[4] such a mechanism is nonetheless likely associated with smaller local conformational changes even though these may not always be observed. Recent advances in protein NMR, molecular dynamics (MD) simulations, and isothermal titration calorimetry (ITC) have illustrated that subtle changes in dynamic fluctuations of proteins can govern the communication of allosteric information between distant sites without major conformational change, and that even intrinsic disorder and local unfolding can play an important role in allosteric regulation, thereby confirming the role of dynamics in allostery (ref 5 and references therein).

This concept of dynamic allostery is receiving increasing recent attention.[5−7] However, understanding how the allosteric signal is communicated at an atomic level between distant sites remains challenging, due to the subtle, transient, and complex changes in dynamics encountered during entropically driven allosteric regulation. It is now well accepted that the allosteric signal is propagated via multiple pathways through a network of physically and/or thermodynamically interconnected residues.[8−10] Allosteric ligand binding perturbs this communication network and results in a functional response by the protein.

However, elucidating such communication networks remains elusive, as they cannot be readily recognized by large changes in residue interactions and may include entropic (hydrophobic interactions, and changes in protein flexibility) as well as enthalpic (van der Waals, hydrogen bonding, and Coulombic interactions) effects. Hence, the most recent approaches take advantage of MD simulations and aim to identify and characterize these allosteric networks[11] using correlation analysis of residue−residue contacts,[12] dynamical network models,[13,14] force distribution analysis,[15,16] degree of frustration,[17] evolutionary covariance,[18] or correlated motions using

Received: December 15, 2015
Published: January 21, 2016

DOI: 10.1021/jacs.5b13134
J. Am. Chem. Soc. 2016, 138, 2036−2045

mutual information theory.[19,20] These approaches provide complicated communication networks that often need to be coarse-grained for analysis, leading to the loss of atomic-level details. This results in the omission of electrostatic effects during analysis despite their potential influence.[11] Moreover, experimental validation of these reconstructed networks is uncommon, due to their complexity.

Here we propose and test an approach that relies on the analysis of pK_a variations of ionizable residues during MD simulations as a means of capturing the allosteric communication pathway. The pK_a of ionizable residues is neither fixed nor constant in time, but rather depends on their local environment and dynamics.[21] Therefore, substantial change in the time-averaged pK_a of a given residue upon binding an allosteric ligand suggests that this particular residue or its neighbors may play a role in the allosteric regulation of the enzyme. This approach has the marked advantage of taking into account backbone motions, side-chain fluctuations, solvent exposure, hydrogen bonding, and other electrostatic interactions, which are otherwise difficult to consider individually. The resulting global pK_a metric can be easily deconvoluted to account for the contribution of individual components, and to provide a means to probe dynamic allostery. This approach leads to experimentally verifiable predictions due to the possibility of perturbing a communication pathway by either mutating an ionizable residue or changing the working pH.

To demonstrate the benefits of such an approach, we have used this method to shed light on the allosteric communication pathway of 3-deoxy-D-*arabino*-heptulosonate 7-phosphate synthase from the pathogen *Neisseria meningitidis* (*Nme*-DAH7PS). This enzyme catalyzes the first committed step of the shikimate pathway in bacteria, responsible for aromatic amino acid biosynthesis, and is allosterically regulated by the pathway end-product phenylalanine.[22] As congruent solution-state and crystalline-state structural data were available,[22] *Nme*DAH7PS was selected as a representative example of a group of DAH7PS enzymes, including those from *Escherichia coli*[23] and *Saccharomyces cerevisiae*,[24] that do not undergo major domain changes in response to the binding of a single allosteric ligand. As such, the mechanism of allosteric response and the atomistic communication between active and allosteric sites is particularly challenging to delineate for this group of DAH7PS. Instead of large-scale domain movements, regulation appears to be mediated by changes in the noncovalent interactions upon binding of the allosteric effector, phenylalanine (Phe), resulting in subtle fluctuations in dynamics and conformation at the active site. By tracking the pK_a changes and fluctuations associated with this allosteric effector, our study illuminates a dynamic network of noncovalent interactions that affects primarily the dynamics of the protein to ultimately regulate its catalytic activity.

RESULTS

Comparison of Phe-Bound and Phe-Free Structures Implicates a Hydrogen-Bonding Network in the Allosteric Response. DAH7PS is a metalloenzyme that catalyzes the condensation of erythrose 4-phosphate (E4P) and phosphoenolpyruvate (PEP) to form DAH7P.[22] PEP binds deep within the active site, located at the C-terminal ends of the beta strands of the $(\beta/\alpha)_8$ barrel, and E4P interacts principally with the residues of the $\beta_2\alpha_2$ loop (Figure 1). *Nme*DAH7PS is homotetrameric, consisting of two pairs of active, regulated dimers[25] that share an extensive interface. There is a single

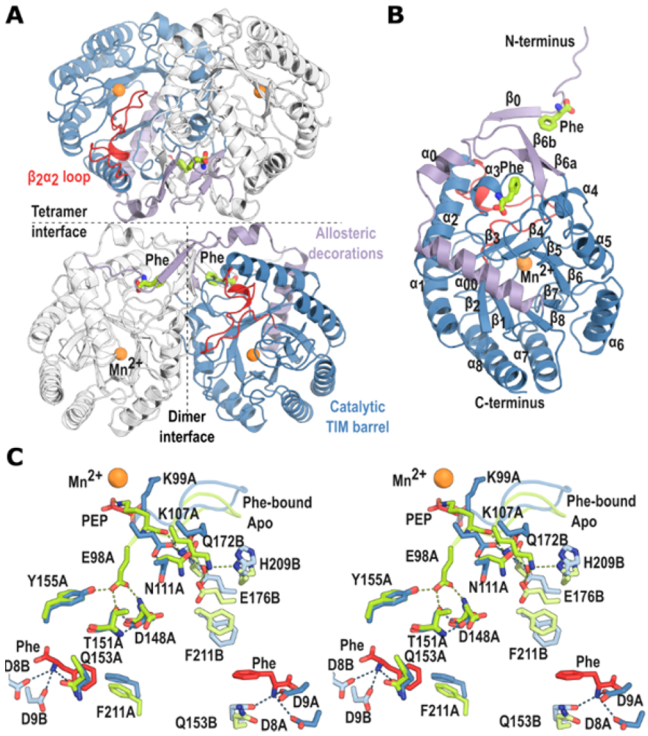

Figure 1. (A) Homotetrameric Phe-bound *Nme*DAH7PS, for each dimer, one chain is displayed in white, while the adjacent chain is colored with the following scheme: main $(\beta/\alpha)_8$ barrel in blue, allosteric decorations in purple, and catalytically important $\beta_2\alpha_2$ loop in red. Mn^{2+} is shown as orange spheres, and Phe as green sticks in each monomeric unit. (B) Monomeric unit of Phe-bound *Nme*DAH7PS with using the same color scheme as described above and with the name of the secondary structure elements displayed. (C) Stereoview of the overlay of the dimer interface of chain A and B of *Nme*DAH7PS for the apo (green) and Phe-bound (blue) forms. Hydrogen bonds are colored with respect to the structure they originate; apo, green; and regulated, blue. Maps showing electron density for bound Phe are shown in Figure S1, and a more detailed view of the active sites of both Phe-bound and Phe-free proteins is shown in Figure S2.

allosteric site per chain, located close to the dimer interface, and the pair of sites is separated by a distance of ~25 Å. The allosteric site is located ~24 Å from its nearest active site, which is on the same chain, and is ~30 Å across the dimer interface from the active site of the opposing chain. The allosteric site is formed in part by an N-terminal extension from the opposing chain, which closes over the allosteric ligand, Phe, and also by the β-hairpin (β_{6a} and β_{6b}) insertion into the $\alpha_5\beta_6$ loop that contributes to the dimer interface (Figure 1A).

A crystal structure of *Nme*DAH7PS bound to allosteric inhibitor Phe was determined at 2.2 Å (PDB code 4UC5). Comparison of this structure with the unliganded structure (PDB code 4HSN)[22] gives a root-mean-square deviation (RMSD) of 0.96 Å for the alignment of 1302 Cα atoms of the tetramer, and 0.583−0.752 Å for the alignment of 639−641 Cα atoms from all dimer pairings. There is an ~2° twist of one dimer relative to the other in the presence of Phe accounting for the larger change observed when the tetramers are compared. Despite the overall similarity between Phe-free and Phe-bound structures, it is evident that localized areas of the protein are displaced in the Phe-bound structure. In particular, the N-terminal extension (residues 1−11) becomes

DOI: 10.1021/jacs.5b13134
J. Am. Chem. Soc. 2016, 138, 2036−2045

ordered around the bound Phe. Additionally, the $\beta_2\alpha_2$ loop (residues 95−120) is repositioned, with an average Cα RMSD from the apo structure of 2.3 Å. This change is associated with some differences in hydrogen-bonding partners for residues of this loop. Hydrogen bonds between Lys107 and residues Glu176, His209, and the backbone carbonyl of His210 of the opposing chain are lost, whereas new hydrogen bonds are established between Lys107 and Glu98 and Gln172 of the opposing chain. Likewise, hydrogen bonds between Glu98 and residues Thr151, Tyr155 and the backbone of Asp148 are lost, as is the hydrogen bond that links the backbone carbonyl of the catalytic Lys99[26] with Gln172 of the opposing chain. The $\beta_2\alpha_2$ loop contributes several residues of importance to substrate binding and catalysis[26] and the local changes in conformation observed in this structure relative to the Phe-free protein are likely to be associated with the changes in catalytic properties observed for this protein in the presence of Phe: a 4-fold reduction in k_{cat} and 2-fold increases of the apparent K_m values for both substrates[22] (Figure S2).

Allosteric Regulation Triggers Local Flexibility Changes and Leads to a Loss of Correlated Motions. To study the dynamics of *Nme*DAH7PS in solution, molecular dynamics (MD) simulations of both the apo and Phe-bound forms of the tetrameric enzyme were conducted in explicit water after modeling of the missing residues from both structures. For each system, two simulation runs of 200 ns were performed starting from slightly different structures (see Methods). As it has recently been demonstrated that the dimer is the elementary biological unit of the enzyme, capable of both catalysis and regulation,[25] analysis of the trajectories has been carried out on the dimeric unit, leading to a combined total of 800 ns simulated for both the apo and Phe-bound dimers.

The root-mean-square deviations (RMSD) of the α-carbons along the trajectories indicate that the simulations can be considered as fully equilibrated after about 80 ns; therefore, the following analyses are conducted on the last 120 ns of each trajectory. The dimers in the presence and absence of Phe sample slightly different, nonoverlapping conformations but do not deviate from their respective crystal structure by more than 3.7 Å (Figure 2A). Overall, the RMSD results indicate that although the active and inhibited forms present a slightly different dynamic profile, both do not undergo large conformational changes or domain motions within the period of analysis and the differences between the apo and Phe-bound states are subtle.

The distribution of the distances between the center of mass of each monomeric unit composing the functional dimer is more narrow in the absence of Phe and has a lower average calculated distance, suggesting a slight increase in dynamics for each chain with respect to the other and a looser association of subunits to form the dimer in the presence of Phe (Figure S3).

α-Carbon root-mean-square fluctuations (RMSF) averaged per chain and per run, reveal only limited differences in the flexibility of the apo and Phe-bound chains, confirming the absence of major conformational changes over the course of the simulation (Figure 2B). Unsurprisingly, the flexibility of the N-terminal tail, which covers the allosteric site upon binding of Phe, is greater for the apo form. This is also the case for the $\alpha_0\alpha_{00}$ loop which comes in contact with the tip of the N-terminal tail in the presence of Phe. Apart from the N-terminal region, the greatest change in observed upon binding of Phe corresponds to key catalytic $\beta_2\alpha_2$ loop, which becomes

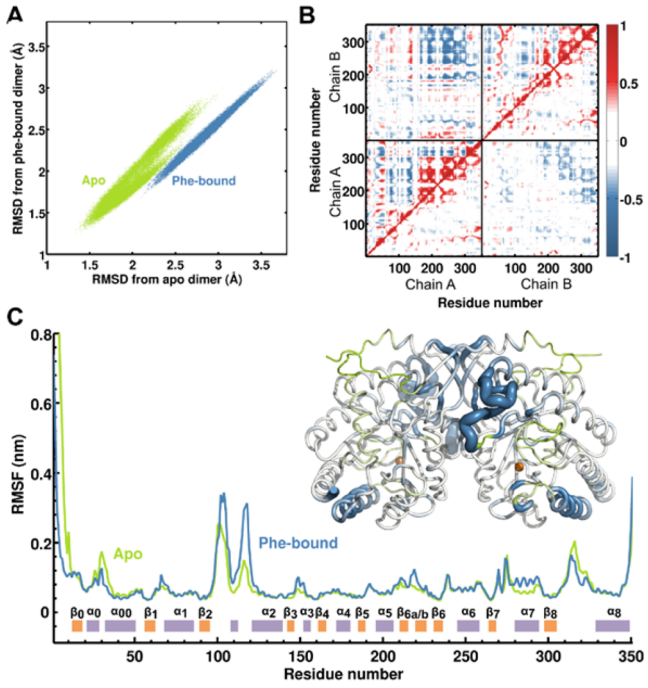

Figure 2. (A) RMSD of the α-carbons of the dimer along the last 120 ns of simulation of each MD runs in the presence (blue dots), absence (green dots) of allosteric Phe, calculated using the X-ray crystal structure of the apo (x coordinates) and Phe-bound (y coordinates) forms as references. (B) Correlations between α-carbons of the dimer calculated using the Pearson coefficient. The upper triangle corresponds to the apo form and the lower triangle to the Phe-bound form. Correlation values are represented by a color gradient of blue to red. Correlated motions with an absolute value below 0.25 are neglected. (C) Cα root-mean-square fluctuations (RMSF) of the apo (green) and Phe-bound (blue). Secondary structure of the monomeric unit is depicted with orange and purple rectangles to identify β-strands and α-helices, respectively. The difference in RMSF between the Phe-bound and apo forms is displayed on the dimer structure. Regions which are more flexible in the presence of Phe are represented with an increased thickness and a blue color gradient while regions more flexible in the apo trajectory are represented with decreased tube diameter and a green color gradient.

significantly more flexible in the presence of the allosteric ligand. These changes in flexibility may account for the changes observed in the conformations of several key residues of this loop in the Phe-bound structure. In addition, binding of Phe leads to an increase in flexibility of the $\beta_3\alpha_3$ loop, β-hairpin insertion, and the region between residues 150 and 180 (β_4 to α_4 region). Finally, the external helix α_7 appears to experience greater fluctuation in the Phe-bound form while the $\beta_8\alpha_8$ loop becomes more rigid.

Overall, both intra- and interchain motions between residues are more correlated in the absence of allosteric inhibitor, as revealed by the normalized matrix of correlated motions between residues obtained from covariance matrix of the α-carbon atoms of each residue. This suggests that, upon binding of Phe, a significant part of the interactions that permit correlation between residues is lost leading to essentially uncorrelated, more random motions, consistent with an entropically driven allosteric mechanism. Moreover, the loss of correlation between residues involved in substrate recognition or catalysis implies that they are not able to work in concert to properly fulfill their purpose, creating an entropic penalty that is manifest in the observed increases in the

DOI: 10.1021/jacs.5b13134
J. Am. Chem. Soc. 2016, 138, 2036−2045

apparent K_m values for substrates PEP and E4P and in the reduction in k_{cat}.

pK_a Analysis Identifies Ionizable Residues Involved in the Allosteric Response. The calculated pK_a values for the ionizable residues of each frame of the apo and Phe-bound trajectories were determined using PROPKA3.1.[27] By taking into consideration all the conformations sampled during the MD simulations, this approach provides a robust means to assess the average pK_a value of a particular residue, how much it fluctuates around this average, and the factors (desolvation effects, hydrogen bonds, and Coulombic interactions) influencing this value.

The differences between the pK_a of the ionizable residues of the apo and Phe-bound forms, averaged over the course of the MD simulations, enable a number of residues likely to be involved in the allosteric communication pathway to be identified. Twelve residues were calculated to experience a significant pK_a shift upon binding of Phe (Figure 3A). These residues are found to be at key positions or to have a specific role (Figure 3B): Lys216 is involved in the binding of allosteric Phe and Lys99 is responsible for proton-transfer reaction within the active site as part of catalysis. Glu98 and Lys107 are found on the $\beta_2\alpha_2$ loop and interact with Asp148, whereas Glu176 interacts with Lys107 across the dimer interface in the apo form. As the backbones of residues Asp148, Tyr155 and Glu176 are relatively close to the allosteric binding sites, they are likely to be affected by the binding of Phe. Tyr26 and His219 are positioned at the tetrameric interface. The predicted pK_a shift of Tyr5 is likely to be due to the alteration in the flexibility of the N-terminal tail.

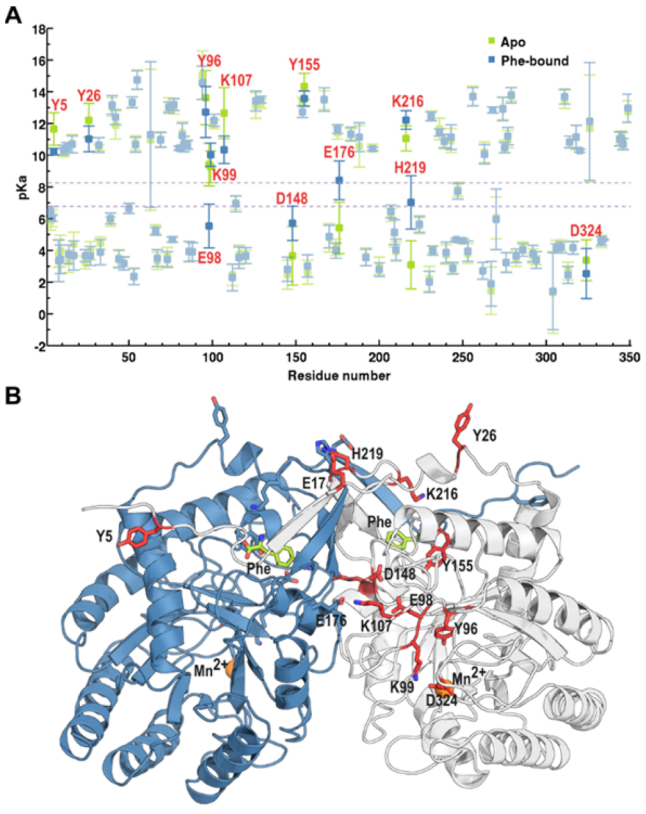

Figure 3. (A) Average pK_a values for the apo and Phe-bound forms are represented with green and blue squares, respectively, while the error bars correspond to ±1 standard deviation around the average. In addition, the differences between the average pK_a values for the apo and Phe-bound forms are presented in Figure S4, while the differences between the standard deviation values are shown in Figure S5. The lowest (6.8) and highest (8.3) experimental pHs used are represented with dotted purple lines. Ionizable residues that present a major pK_a shift upon binding of Phe have their residue number indicated in red while the other ionizable residues appear faded in the background. (B) Structure of the dimer (one chain is shown in blue, the other in white) with residues experiencing major pK_a shifts represented in sticks. The two allosteric sites are highlighted by the presence of Phe shown in green sticks, while the catalytic sites are identified with the manganese ions shown as orange spheres.

The standard deviation of the pK_a values of each ionizable residue over the course of the MD trajectories gives an indication of how much its pK_a value is predicted to fluctuate in the presence or absence of Phe (Figure 3A). These fluctuations may be associated with changes in conformational dynamics for the residue itself or for its surrounding environment. It is also apparent that a shift in the predicted average pK_a value upon binding of Phe is not necessarily associated with a change in calculated pK_a fluctuation, with Glu98 being the best example of such behavior. This observation implies that although the environment of the residue changes in the presence of Phe, this residue remains tightly bound and/or buried in both inhibited and active forms. The opposite behavior is more common; several residues experience a change in the fluctuation of their pK_a value upon binding of Phe, but do not experience any major pK_a shift of their average value. On the other hand, Lys107 experiences a drop in pK_a fluctuations, as well as in pK_a itself, on the binding of Phe.

Interestingly, of the 12 residues for which a major pK_a shift is predicted, Tyr5, Glu98, Lys107, Glu176, and His219 present (almost) no overlap between their values at ±1 standard deviation (Figure 3A), supporting the existence of a significant pK_a difference between the apo and Phe-bound forms. On the other hand, changes in average desolvation are also predicted for Glu98, Lys99, and Lys107 (Figure S6), which experience an increased solvent exposure in the presence of allosteric Phe and for Tyr155, as well as Asp8 and Arg42, which bind allosteric Phe and which become more buried in the presence of Phe.

Inter- and Intrachain Communication Changes upon Allosteric Inhibitor Binding. To identify changes in the hydrogen bonds and Coulombic interactions between pairs of residues upon binding of Phe that are likely to affect the pK_a of ionizable residues, a weighted map of interactions in which two nodes represent two interacting residues and the diameter of the edge linking the two nodes accounts for the strength of the interaction was generated. By specifying the working pH, we can predict which residues are protonated and thus account for the favorable, unfavorable or nonexistent Coulombic interactions depending on the charge borne by the residues (Figure 4A).

The hydrogen bonding and Coulombic interaction maps reveal clearly that in the absence of allosteric inhibitor, the key predicted interactions are the favorable Coulombic interactions between Glu176 and Lys107 across the dimer interface, and between Lys107 and Asp148; the unfavorable ones are between Asp148 and Glu176 across the dimer interface, as well as the hydrogen bond between Asp148 and protonated Glu98 (Figure 4A). These strong interactions ensure close contact between the two chains of the core dimeric unit of the enzyme and provide a short and robust interchain communication pathway between the allosteric site of one chain and the active site of the adjacent chain in the absence of Phe. Upon binding of allosteric

DOI: 10.1021/jacs.5b13134
J. Am. Chem. Soc. 2016, 138, 2036−2045

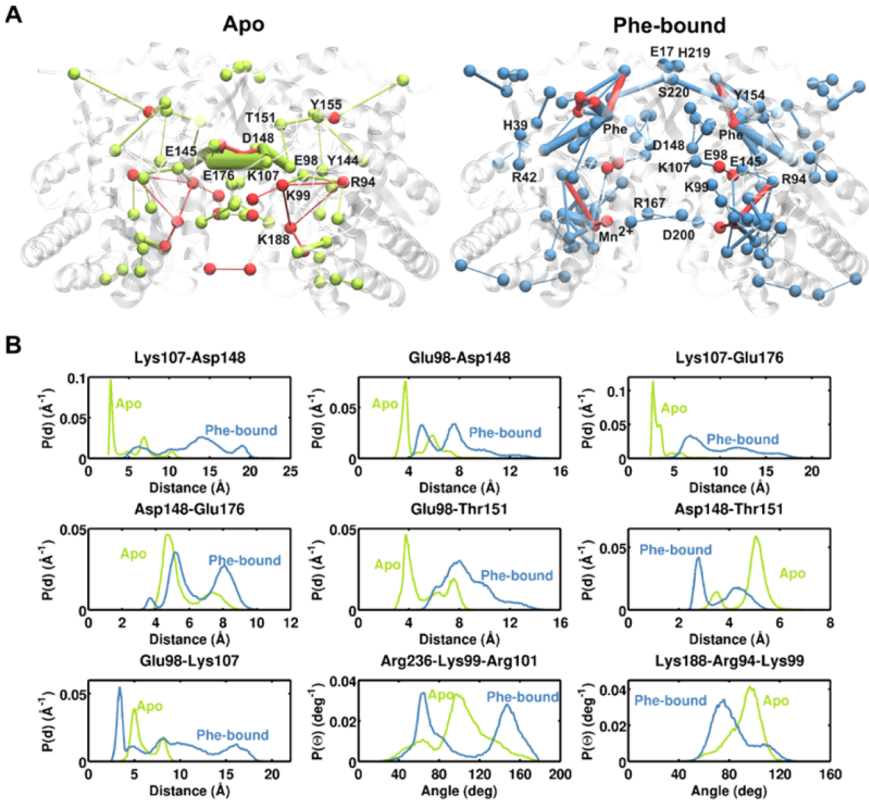

Figure 4. (A) Hydrogen bonds and Coulombic interactions that are only present or are stronger in the apo (left) or the Phe-bound (right) trajectories. Nodes represent interacting residues and the edges between nodes indicate the interactions, with the diameter of the edge accounting for the strength of the interaction. For the apo form, favorable interactions are shown in green and unfavorable ones are in red, and in the Phe-bound form favorable interactions are in blue and unfavorable ones are in red. The contribution of each effect (side chain hydrogen-bond, backbone hydrogen-bond and Coulombic interactions) is detailed in Figure S7. (B) Distribution of the distances between key ionizable groups. Frequency distribution of the distances for the apo (green) and Phe-bound (blue) forms. The distances are calculated using the hydroxyl oxygen of Ser, Tyr, Thr, the center of the two carboxyl oxygens of Glu and Asp, the nitrogen of the ε-amino group of Lys, the center of the guanidinium ion of Arg, and the center of the two nitrogens of the imidazole ring of His.

Phe all these strong interactions are lost, essentially leading to the disruption of the network of interactions between ionizable residues that exists across the two chains (Figure 4A). This observation is confirmed by examining the calculated distance distributions between the ionizable groups of these residues over the course of the MD simulations (Figure 4B). The calculated distance of 2.7 Å between Lys107 and Asp148 in the apo form is shifted to 6−19 Å in the presence of Phe, whereas the distance between Glu98 and Asp148 changes from 3.7 Å in the apo form to around 5 Å. The distance between Glu176 and Lys107 across the tight dimer interface is mainly centered around 2.7 and 3.5 Å in the absence of ligand, but is not closer than 5 Å and is calculated to reach as much as 18 Å in the presence of the allosteric ligand. Finally, the distance between the two negatively charged residues Glu176 and Asp148 in the apo form across the interface remains centered around 4.6 Å (Figure 4B), whereas binding of Phe and protonation of Glu176 enables this distance to reduce to as little as 3.6 Å between the two ionizable groups, although the distances are mainly centered around 5.2 and 8 Å.

Within a single chain of the unregulated enzyme, Tyr155, which is close to the allosteric site, interacts via a hydrogen bond with Thr144 (adjacent to catalytically important Glu145) and with Thr151, which in turn interacts with Glu98. These interactions, which are lost upon binding of Phe, may contribute to communicate the allosteric information within a single chain. In the presence of Phe, the distance between Glu98 and Thr151 increases, while the distance between Thr151 and Asp148 decreases with the pair interacting via a hydrogen bond (Figure 4B). Binding of Phe also leads to the formation of strong interactions within and around the allosteric site, which tighten the upper part of the dimer.

A number of important changes also occur within and around the active site. In the apo form, repulsive Coulombic interactions exist between catalytically important residues Lys188 and Lys99, both of which are involved in the proton-transfer mechanisms during catalysis, Arg94 which binds the carboxylate of PEP, as well as Arg236 and Arg101 which bind the phosphate of PEP and E4P respectively.[26] This network of interactions among positively charged residues, which is only present in the absence of Phe, is likely to maintain the correct relative distances between key residues, thereby maintaining the most catalytically active conformation. Additionally, Glu145 interacts more favorably with Lys99 and Arg94 in the absence of Phe. Binding of Phe reshuffles this interaction network, whereby Lys107 and Glu98 now interact via a hydrogen bond and move closer to one another with a distance of 3.4 Å, compared with 5 Å in the absence of ligand (Figure 4B). The negative charge on Glu98 has an unfavorable effect on Glu145, which interacts less with Arg94 and Lys99, such that the functional groups of these two residues move away from Glu145. The slight balance of repulsive charge−charge interactions between catalytically important Lys99, Lys188, and Arg94 is also broken, and the distances between the

DOI: 10.1021/jacs.5b13134
J. Am. Chem. Soc. 2016, 138, 2036−2045

functional groups of these residues increase. Significant changes in the angle formed by the functional groups of these interacting residues also support a shift from an active to an inactive topology of the key catalytic residues upon binding of Phe (Figure S8). Finally a large number of existing interactions centered on the metal ion are significantly strengthened in the presence of Phe.

The Inhibitory Effect of Allosteric Phe Is Reduced at Elevated pH. The pK_a calculations of the regulated and apo forms of *Nme*DAH7PS exposed several residues that likely adopt significantly altered pK_a values in the presence and absence of Phe (Figure 3A). Of particular interest are Glu98 and Glu176, which both present unusually high pK_a values for Glu and are predicted to have different protonation states at standard assay pH depending on the presence of Phe. At an assay pH of 6.8 Glu98 is predicted to be protonated in the apo enzyme and deprotonated in the Phe-bound form, whereas Glu176 is predicted to be deprotonated in the apo form, but protonated in the presence of Phe. As the pK_a values of these residues may lie close to assay pH, changing their protonation state experimentally through variations in pH may mimic in part the allosteric response.

To investigate the pH-dependence of activity and allosteric response, assays were conducted between pH 6.8 and 8.3, as enzyme activity is observable within this pH range. Outside this range, the protonation states of the substrates and important catalytic residues may be affected. Based on the pK_a analysis, only Glu176 in the presence of Phe is predicted to undergo a change in protonation state on increasing the pH over this range. In this case, since the pK_a = 8.4 ± 1.2, only a partial deprotonation of Glu176 occurs at pH 8.3. Glu176 in the apo form, however, should not experience changes in its protonation state over this pH range,(pK_a = 5.4 ± 1.6). Moreover, Glu98 is not predicted to be affected significantly in this pH range, both in the presence and absence of Phe, where, respectively, Glu98 remains deprotonated (pK_a = 5.5 ± 1.4) and protonated (pK_a = 9.4 ± 1.3).

Therefore, the transition from a deprotonated to a protonated state for Glu176 that occurs at pH 6.8 upon binding of Phe will not occur to the same extent at higher pH. Consequently, by increasing the pH, the proportion of deprotonated Glu176 is expected to increase, leading to the partial restoration of the major Coulombic interaction between Glu176 and Lys107. Thus, at high pH a lower level of inhibition in the presence of Phe is expected than at low pH.

In the absence of Phe, the specific activity was observed to decrease only slightly between pH 6.8 and 7.8, with a sharper reduction at pH 8.3 (to 90% of maximal activity, Figure 5A). More importantly, in the presence of Phe the inhibitory response was observed to be severely attenuated as the pH was raised (Figure 5A). This is in complete agreement with the effect of a reduced fraction of protonated Glu176. Comparable K_D values were measured by isothermal titration calorimetry (ITC) for the binding of Phe at both pH 7 and pH 7.8 (the maximum pH for enzyme stability over the course of this experiment), indicating that the binding of Phe is not compromised in this pH range. Moreover, the entropic and enthalpic contributions to the free energies of binding of Phe to each site in the sequential two-site binding model are very similar at both pH values (Figure 5B). These results are consistent with the dependence of *Nme*DAH7PS allostery on the network of ionizable residues for signal transmission. It is also noted that two significantly different binding constants for

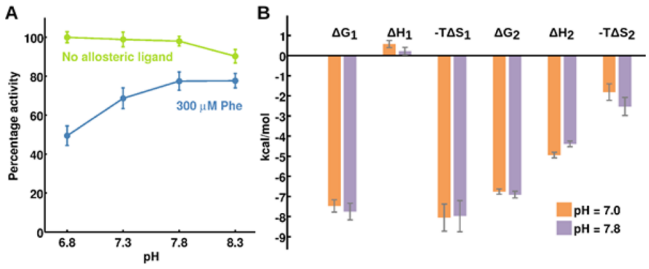

Figure 5. (A) Effect of pH on the activity and inhibition of *Nme*DAH7PS in the presence of 300 μM L-phenylalanine. Activity at varying pH compared to maximal activity seen at pH 6.8 (green line). Activity at varying pH in the presence of 300 μM Phe compared to uninhibited enzyme at pH 6.8 (blue line). Substrate concentrations were at least 5-fold higher than the K_m values (assessed at the different pH values) of each substrate at each pH (substrate concentrations were 100 μM PEP and 500 μM E4P). (B) Entropic and enthalpic contributions to the binding isotherm of Phe to *Nme*DAH7PS at pH 7 (orange) and pH 7.8 (purple).

Phe observed by ITC (Table S1), support the calculations that predict communication across the dimer interface.

DISCUSSION

Evolution has favored the existence of subtle yet fundamental, dynamic networks of noncovalent interactions within proteins that are intimately related to function. These noncovalent interactions consist primarily of hydrogen bonds and Coulombic interactions but also involve hydrophobic interactions and water-mediated hydrogen bonding. As a protein samples its energy landscape, interactions between residues that comprise the network are constantly changing. A method of altering the dynamics of a protein and therefore its function is to alter the existing network by favoring transient, noncovalent interactions through the binding of an allosteric effector molecule in order to reshape the conformational space sampled by the protein. This altered state will manifest as the product of the interactions broken and formed in the network linking the two remote sites. In order for the information from a remote site to be conferred to the active site, communication through these complex noncovalent bonding networks is essential.

Allosteric regulation of *Nme*DAH7PS relies on changes in the intricate network of interactions that connect allosteric and catalytic sites of the protein, both within a single chain and across the dimer interface. This network undergoes a significant reorganization to evoke the allosteric regulatory response in the enzyme. For the apo enzyme this network enables the communication between the allosteric site and the catalytic site through the dimer interface in particular via strong Coulombic forces among Glu98, Lys107, Asp148, and Glu176, but also within a single chain via hydrogen bonds involving Thr151, Tyr155, Glu145, and Glu98. The presence of the allosteric effector molecule Phe, leads to the loss of these two communication pathways between allosteric and active sites and an increase in noncorrelated motions within the enzyme. The catalytic activity of the enzyme appears to be considerably lowered mainly because of the increased flexibility of the $\beta_2\alpha_2$ loop, providing an entropic penalty to substrate binding, and disruption of the optimal, finely tuned, relative position of key catalytic residues, providing a primarily enthalpic penalty to substrate binding.

Identification of the changes occurring in the reorganization of this network is revealed by monitoring the calculated pK_a

DOI: 10.1021/jacs.5b13134
J. Am. Chem. Soc. 2016, 138, 2036−2045

variability between the active and regulated forms during the course of a MD simulation. Previous similar studies have, however, been made on a limited selection of structures generated from MD to depict protein flexibility.[28−35] Our studies show that the use of comprehensive sampling of conformational space leads to the complete recovery of the vast information pK_a calculations can provide and enable the formulation of robust conclusions based on the observed variations.

In principle, constant-pH molecular dynamics (CpHMD)[36−38] should be the method of choice for studying pK_a variations as a function of protein motions. However, such an approach cannot be applied as an analytical tool on existing trajectories and is usually associated with a computationally expensive replica-exchange method that cannot be applied to large multimeric proteins. Apart from CpHMD, the pK_a of ionizable residues in a protein can be assessed using either methods that relies on the Poisson−Boltzmann[39] or Generalized Born[40] continuum models (which are, for example, implemented in MEAD,[41] MCCE,[42] pkD,[43] UHBD,[44] and H++[45]); or empirical methods such as implemented in PROPKA.[27] PROPKA has been shown to outperform electrostatic based methods[27] while reducing computational cost and is thus well suited for performing pK_a analysis of complete, existing MD trajectories.

It should be emphasized that the key residues that are predicted to play an important role in the signal transmission are not readily identified by comparing the pK_a or structural changes of the crystal structures (Figure S9). Indeed, not surprisingly such an approach is precluded by the inherent static image of the interactions. For instance, Gln172, His209, Asn111, and Arg175 are deemed important from structural analysis whereas MD analysis revealed the minor contribution of these residues to allostery. Similarly, the importance of Glu176, Tyr155 and Thr151 could only be illuminated by the MD simulations. Solely relying on the pK_a difference between apo and Phe-bound crystal structures (Figure S9) leads to a number of "false positives" and to the oversight of key residues such as Asp148 and Lys107. Within the active site, changes in the conformation of Lys99, Arg167, and Arg101 are indeed observed; however, changes to the important catalytic residue Lys188 and to the PEP-binding residues Arg94 and Arg236 are only revealed through the MD simulations. Combining structural analysis, MD simulations and pK_a analysis of the MD trajectories therefore greatly improves the robustness of the results and enables the interpretation of the findings to be refined and to lead to experimentally verifiable results.

Notwithstanding the relative small overall free energy differences (3−5 kJ mol^{-1}) associated with changes to K_m(E4P), K_m(PEP) and k_{cat} on binding the allosteric effector Phe, substantial local changes are observed in the molecular dynamics simulations of the protein, within and between subunits and propagating to the active site. These changes can be conveniently monitored through changes in pK_a values of ionizable residues and changes in the distribution of pK_a values about their respective means. Changes in the pK_a of ionizable residues result from distinct changes in the noncovalent interaction network connecting the functional sites of *Nme*DAH7PS. We have shown that alteration of the protonation state of these crucial ionizable residues by altering the pH limits the ability of the enzyme to effectively reorganize its interaction network in the presence of Phe.

The combination of MD and pK_a calculations exposes the communication network between functionally important remote sites. The methodology described here to illustrate the complexities of "dynamic allostery" can be transferred to any enzyme that is likely to rely on subtle short time-scale changes in dynamics and networks of noncovalent interactions between residues for activation, regulation, and complex formation.

CONCLUSION

Allostery is the process by which binding of a ligand at one site of a protein leads to a functional response at a distant site. Despite its importance in enzymatic regulation, little is known about how the allosteric signal is communicated from one site to the other, especially in the absence of large conformational changes in the protein. Here we have shown that monitoring the pK_a variations of ionizable residues over the course of molecular dynamics simulations in the presence and absence of allosteric regulator can unravel the allosteric communication pathways in proteins. We have verified the predictions of this approach experimentally, by showing that subtle pH variations can mimic the allosteric control, by changing the protonation state of key residues without affecting the catalytic activity of the enzyme or its ability to bind an allosteric effector molecule. This method can be applied to identify changes in a network of noncovalent interactions occurring between the distinct states of any protein.

METHODS

Crystallization of *Nme*DAH7PS. *Nme*DAH7PS was expressed and purified as previously described.[22] The resulting protein solution was concentrated to approximately 10 mg mL^{-1}. Then 1 μL of enzyme solution (9−11 mg mL^{-1}) was mixed with 1 μL of crystallization buffer containing 0.1 M Tris HCl (pH 7.3), 0.2 M trimethylamino-*N*-oxide (TMAO), 600 μM $MnSO_4$, and 15−20% (w/v) PEG 2000MME. Crystals were grown by hanging drop vapor diffusion over 500 μL of crystallization buffer, and the crystallization trays were incubated at 20 °C. Crystals began to form in 48 h and were fully formed within 7 days. The grown crystals were added to another drop containing 50% SEC buffer containing 200 μM PEP, 100 mM KCl, and 10 mM BTP and 50% crystallization buffer also containing 10 mM Phe and left to soak for 2−6 h. Crystals were flash frozen using liquid nitrogen in a cryoprotectant solution containing ligand present reservoir solution and 20% (v/v) PEG400.

Crystallography, Structure Determination, and Refinement. An X-ray diffraction data set was collected at the Australian synchrotron using the MX1 beamline.[46] The data sets were integrated and processed using XDS and AIMLESS.[47,48] Appropriate cutoff resolution was determined via $CC^{1/2} \geq 0.5$ ensuring the data were complete in the highest resolution shell.[49] Space group and unit cell parameters for *Nme*DAH7PS with the soaked ligands were the same as those previously identified (PDB code 4HSN),[22] meaning that initial phases could be obtained via molecular replacement using the original structure as a search model in Phaser MR.[50] All ligands and waters were removed from the search model (PDB code 4HSN) before molecular replacement was carried out. Refmac5 was used to generate the electron density map and this was manually analyzed and refined in COOT.[51,52] The quality of the model was optimized by consecutive model building in COOT and refinement with Refmac5. Water molecules were added manually via interpretation of the ($|2F_0| - |F_c|$) map ensuring that they had the ability to hydrogen bond to at least one acceptor or donor. Residues Met1-Asp9 were absent from the model (PDB code 4HSN) used for molecular replacement; however, this region of the protein becomes ordered in the presence of Phe and only the first three residues remain unresolved. Molprobity was used to assess structure quality during refinement cycles and before

DOI: 10.1021/jacs.5b13134
J. Am. Chem. Soc. 2016, 138, 2036−2045

deposition.[53] Diffraction data and refinement statistics are provided in Table S2. The Phe-bound structure is deposited as 4UC5.

Isothermal Titration Calorimetry. Binding of *Nme*DAH7PS to L-phenylalanine at pH 7 and 7.8 was measured by ITC using a VP-ITC unit operating at 298 K (MicroCal, GE Healthcare). Before use, the protein was buffer exchanged against binding buffer [0.5 mM MnSO4 in 50 mM BTP buffer (pH 7 and 7.8)] and all solutions were degassed in a vacuum. Protein concentration was measured by UV absorption immediately before titrations were started. The titrations were composed of 28 injections, one 2 μL injection, followed by 27 10 μL injections of L-phenylalanine. The initial datum point was routinely deleted to allow for diffusion of ligand across the needle tip during the equilibration period. A heat of dilution experiment was measured independently and subtracted from the integrated data before curve fitting in Origin 7.0. For the binding of NmeDAH7PS to L-phenylalanine, 15 μM *Nme*DAH7PS was used, and the syringe contained 1.2 mM L-phenylalanine; and the data were fitted with the two-site sequential-binding model supplied by MicroCal. Binding data are summarized in Table S1.

pH Dependent Kinetics. The assay system for *Nme*DAH7PS was a modified form of the assay used by Schoner and Herrmann as previously described.[54] The assays to determine the optimum pH of *Nme*DAH7PS activity contained PEP (100 μM) and $MnSO_4$ (100 μM) in 50 mM BTP buffer, 10 μM ethylenediaminetetraacetic acid (EDTA), and E4P (500 μM) which were the correct pH (6.8, 7.3, 7.8, and 8.3) at 298 K. Outside of this range, the enzyme dramatically lost activity. The buffer was made up in ultrapure water that had been treated with Chelex resin. After incubation at the required temperature for 5 min, the reaction was initiated by the addition of enzyme (2 μL, 1.0 mg/mL). For the pH dependent inhibition kinetics, the buffer contained the same components as above, except 300 μM L-phenylalanine was added before incubation. All assay experiments were performed in triplicate.

Confirmation that Substrate Binding Was Not Severely Affected by pH Range. For *Nme*DAH7PS at pH 8.3, the reactions to determine K_m^{E4P} used 100 μM PEP and 32−375 μM E4P, and for K_m^{PEP} used 500 μM E4P and 3−100 μM PEP. For *Nme*DAH7PS at pH 6.8, the reactions to determine K_m^{E4P} used 100 μM PEP and 12.5−250 μM E4P, and for K_m^{PEP} used 500 μM E4P and 7.5−120 μM PEP. The buffers contained $MnSO_4$ (100 μM) in 50 mM BTP buffer and 10 μM ethylenediaminetetraacetic acid (EDTA). They were initiated by the addition of *Nme*DAH7PS (2 μL, 1.0 mg/mL). K_m^{E4P} and K_m^{PEP} at pH 6.8 and 8.3 are summarized in Table S3.

System Preparation for the MD Simulations. The crystal structures of *Nme*DAH7PS in the absence (PDB ID: 4HSN) and presence of allosteric Phe (PDB ID: 4UC5) were used as a starting point for the calculations. Missing residues and side chains were reconstructed with MODELLER.[55] The top two tetrameric models generated for each structure, selected on the basis of the lowest MODELLER objective function value and the lowest global DOPE score, were chosen as starting point for the simulations (two simulations for each apo and Phe-bound forms). PROPKA3.1[27] was used to assess the pK_a of ionizable residues and the value averaged by chain and model. The protonation state of these residues for the apo system and for the Phe-bound system was then selected based on these pK_a to simulate a pH of 7.3. Proton position of histidine residues was chosen with MCCE.[42]

MD Simulations. All MD simulations were carried out with NAMD[56] using CHARMM all-atom parameter set 22 with the CMAP Correction.[57,58] The simulations were run on 1048 cores of the IBM BlueGene/P part of the high performance computing service facility at the University of Canterbury. The particle mesh Ewald (PME) method was used to calculate electrostatic interactions and van der Waals cutoff was set up at 12 Å. Each system was solvated in an explicit TIP3P water box of 118 Å × 118 Å × 130 Å, and the net charge neutralized with Na^+ and Cl^- ions added with a minimum distance of 5 Å from the enzyme and from each other. Using the conjugate gradient energy minimization method, each solvated protein was minimized for a total of 100 000 steps first by allowing only water molecules, ions, and hydrogens atoms to move (20 000 steps), then keeping only the backbone atoms fixed (30 000 steps) and finally releasing all atoms (50 000 steps). Each system was then gradually heated from 0 to 310 K over 124 000 steps keeping a harmonic restraint of 10 kcal/mol on backbone atoms. The Nosé−Hoover Langevin piston pressure control was then used to simulate the NPT ensemble at 1 atm, 310 K. Each system was equilibrated for 100 000 steps with the restraint decreased to 5 kcal/mol, for another 100 000 steps with the restraint at 1 kcal/mol, and finally for 1 ns without any restraints. The four equilibrated systems were then each subjected to 200 ns of NPT molecular dynamics simulation at 1 atm and 310 K with the trajectory saved every 10 ps.

Trajectory Analysis. The resulting trajectories were aligned to remove any undesired rotational and translational movements of the enzyme. The first 80 ns of each simulation were removed to allow for full equilibration of the systems. Since it has been shown that the dimeric unit is the smallest biological unit capable of both catalysis and allosteric regulation,[25] so each dimer of the tetramer were considered as two different trajectories for the purpose of position and distance analysis and combined to effectively lead to 480 ns of fully equilibrated trajectory for each system. After alignment of the resulting trajectories, root-mean-square deviations (RMSD) and root-mean-square fluctuations (RMSF) were calculated using Gromacs 4.5.[59] Correlated motions based on Pearson coefficient were determined with Carma.[60] Distance distributions were calculated in VMD[61] using in-house Tcl scripts using the hydroxyl oxygen of Ser, Tyr, Thr, the center of the two carboxyl oxygens of Glu and Asp, the nitrogen of the ε-amino group of Lys, the center of the guanidinium ion of Arg, and the center of the two nitrogens of the imidazole ring of His.

pK_a Analysis. For each frame of the tetramer trajectories, the coordinates of the protein without hydrogen atoms, in complex with its ligands (manganese ions and, should it be present, allosteric Phe) were saved as a PDB format. The resulting files were converted from CHARMM PDB format to a more standard PDB format. For each system, PROPKA3.1 was run on each of the 24 000 structure files in parallel using asynchronous dynamic load balancing and the output files parsed in usable data. In order to take full advantage of the different conformational space sampled by each monomeric unit composing the tetramer, the values of interest (pK_a, desolvation effect) and each type of interaction (Coulombic, side-chain hydrogen bonds, and backbone hydrogen bonds) were analyzed in such way that average values can be obtained (i.e., does not depend on the chain the ionizable residue belongs to). Parsing and analysis of the data were performed using dedicated python scripts. The method and the associated scripts can be easily be transferred to the analysis of other systems and are available upon request.

■ ASSOCIATED CONTENT

Supporting Information

The Supporting Information is available free of charge on the ACS Publications website at DOI: 10.1021/jacs.5b13134.

Supplementary information includes Tables S1−S3 and Figures S1−S7 providing Phe binding constants, X-ray data collection and refinement data, kinetic parameters, difference maps for Phe binding, pK_a differences and detailed maps of the residue interactions (PDF)

■ AUTHOR INFORMATION

Corresponding Author

*emily.parker@canterbury.ac.nz

Author Contributions

‖E.J.M.L. and L.C.H. contributed equally.

Notes

The authors declare no competing financial interest.

DOI: 10.1021/jacs.5b13134
J. Am. Chem. Soc. 2016, 138, 2036−2045

■ ACKNOWLEDGMENTS

This work was funded by the New Zealand Marsden fund (UOC1105). Part of this work is funded by UC HPC, the high performance e-research computing service facility of the University of Canterbury. E.J.M.L. is the recipient of a UC BlueFern HPC PhD Scholarship. L.C.H. is the recipient of a Biomolecular Interaction Centre PhD scholarship. Part of this research was undertaken on the MX1 and MX2 beamlines at the Australian Synchrotron, Victoria, Australia, with usage administered by the NZSG. The authors would like to acknowledge Dr. Jane Allison for stimulating discussions and Dr. Sung Bae for his help in writing some of the python scripts used in this work.

■ REFERENCES

(1) Monod, J.; Wyman, J.; Changeux, J. P. *J. Mol. Biol.* **1965**, *12*, 88.
(2) Koshland, D. E., Jr.; Nemethy, G.; Filmer, D. *Biochemistry* **1966**, *5*, 365.
(3) Cooper, A.; Dryden, D. T. F. *Eur. Biophys. J.* **1984**, *11*, 103.
(4) Nussinov, R.; Tsai, C.-J. *Curr. Opin. Struct. Biol.* **2015**, *30*, 17.
(5) Motlagh, H. N.; Wrabl, J. O.; Li, J.; Hilser, V. J. *Nature* **2014**, *508*, 331.
(6) Kern, D.; Zuiderweg, E. R. *Curr. Opin. Struct. Biol.* **2003**, *13*, 748.
(7) Cui, Q.; Karplus, M. *Protein Sci.* **2008**, *17*, 1295.
(8) Goodey, N. M.; Benkovic, S. J. *Nat. Chem. Biol.* **2008**, *4*, 474.
(9) Tsai, C. J.; Del Sol, A.; Nussinov, R. *Mol. BioSyst.* **2009**, *5*, 207.
(10) Smock, R. G.; Gierasch, L. M. *Science* **2009**, *324*, 198.
(11) Feher, V. A.; Durrant, J. D.; Van Wart, A. T.; Amaro, R. E. *Curr. Opin. Struct. Biol.* **2014**, *25*, 98.
(12) Johnson, Q. R.; Lindsay, R. J.; Nellas, R. B.; Fernandez, E. J.; Shen, T. *Biochemistry* **2015**, *54*, 1534.
(13) Sethi, A.; Eargle, J.; Black, A. A.; Luthey-Schulten, Z. *Proc. Natl. Acad. Sci. U. S. A.* **2009**, *106*, 6620.
(14) Vanwart, A. T.; Eargle, J.; Luthey-Schulten, Z.; Amaro, R. E. *J. Chem. Theory Comput.* **2012**, *8*, 2949.
(15) Palmai, Z.; Seifert, C.; Grater, F.; Balog, E. *PLoS Comput. Biol.* **2014**, *10*, e1003444.
(16) Zhou, J.; Bronowska, A.; Le Coq, J.; Lietha, D.; Grater, F. *Biophys. J.* **2015**, *108*, 698.
(17) Ferreiro, D. U.; Hegler, J. A.; Komives, E. A.; Wolynes, P. G. *Proc. Natl. Acad. Sci. U. S. A.* **2011**, *108*, 3499.
(18) Suel, G. M.; Lockless, S. W.; Wall, M. A.; Ranganathan, R. *Nat. Struct. Biol.* **2003**, *10*, 59.
(19) McClendon, C. L.; Friedland, G.; Mobley, D. L.; Amirkhani, H.; Jacobson, M. P. *J. Chem. Theory Comput.* **2009**, *5*, 2486.
(20) Lange, O. F.; Grubmuller, H. *Proteins: Struct., Funct., Genet.* **2006**, *62*, 1053.
(21) Pace, C. N.; Grimsley, G. R.; Scholtz, J. M. *J. Biol. Chem.* **2009**, *284*, 13285.
(22) Cross, P. J.; Pietersma, A. L.; Allison, T. M.; Wilson-Coutts, S. M.; Cochrane, F. C.; Parker, E. J. *Protein Sci.* **2013**, *22*, 1087.
(23) Shumilin, I. A.; Kretsinger, R. H.; Bauerle, R. H. *Structure* **1999**, *7*, 865.
(24) Hartmann, M.; Schneider, T. R.; Pfeil, A.; Heinrich, G.; Lipscomb, W. N.; Braus, G. H. *Proc. Natl. Acad. Sci. U. S. A.* **2003**, *100*, 862.
(25) Cross, P. J.; Heyes, L. C.; Zhang, S.; Nazmi, A. R.; Parker, E. J. *PLoS One* **2016**, DOI: 10.1371/journal.pone.0145187.
(26) Heyes, L. C.; Reichau, S.; Cross, P. J.; Jameson, G. B.; Parker, E. J. *Bioorg. Chem.* **2014**, *57*, 242.
(27) Olsson, M. H. M.; Søndergaard, C. R.; Rostkowski, M.; Jensen, J. H. *J. Chem. Theory Comput.* **2011**, *7*, 525.
(28) Zhou, H. X.; Vijayakumar, M. *J. Mol. Biol.* **1997**, *267*, 1002.
(29) Soares, T. A.; Lins, R. D.; Straatsma, T. P.; Briggs, J. M. *Biopolymers* **2002**, *65*, 313.
(30) Sandberg, L.; Edholm, O. *Biophys. Chem.* **1997**, *65*, 189.
(31) van Vlijmen, H. W.; Schaefer, M.; Karplus, M. *Proteins: Struct., Funct., Genet.* **1998**, *33*, 145.
(32) Koumanov, A.; Karshikoff, A.; Friis, E. P.; Borchert, T. V. *J. Phys. Chem. B* **2001**, *105*, 9339.
(33) Livesay, D. R.; Jacobs, D. J.; Kanjanapangka, J.; Chea, E.; Cortez, H.; Garcia, J.; Kidd, P.; Marquez, M. P.; Pande, S.; Yang, D. *J. Chem. Theory Comput.* **2006**, *2*, 927.
(34) Whalen, K. L.; Tussey, K. B.; Blanke, S. R.; Spies, M. A. *J. Phys. Chem. B* **2011**, *115*, 3416.
(35) Costa, M. G. S.; Batista, P. R.; Shida, C. S.; Robert, C. H.; Bisch, P. M.; Pascutti, P. G. *BMC Genomics* **2010**, *11*, S5.
(36) Baptista, A. M.; Teixeira, V. H.; Soares, C. M. *J. Chem. Phys.* **2002**, *117*, 4184.
(37) Lee, M. S.; Salsbury, F. R.; Brooks, C. L. *Proteins: Struct., Funct., Genet.* **2004**, *56*, 738.
(38) Meng, Y.; Roitberg, A. E. *J. Chem. Theory Comput.* **2010**, *6*, 1401.
(39) Bashford, D.; Karplus, M. *Biochemistry* **1990**, *29*, 10219.
(40) Kuhn, B.; Kollman, P. A.; Stahl, M. *J. Comput. Chem.* **2004**, *25*, 1865.
(41) Bashford, D. In *Scientific Computing in Object-Oriented Parallel Environments*; Ishikawa, Y., Oldehoeft, R., Reynders, J. W., Tholburn, M., Eds.; Springer: Berlin, Heidelberg, 1997; Vol. *1343*, p 233.
(42) Song, Y.; Mao, J.; Gunner, M. R. *J. Comput. Chem.* **2009**, *30*, 2231.
(43) Tynan-Connolly, B. M.; Nielsen, J. E. *Nucleic Acids Res.* **2006**, *34*, W48.
(44) Madura, J. D.; Briggs, J. M.; Wade, R. C.; Davis, M. E.; Luty, B. A.; Ilin, A.; Antosiewicz, J.; Gilson, M. K.; Bagheri, B.; Scott, L. R.; McCammon, J. A. *Comput. Phys. Commun.* **1995**, *91*, 57.
(45) Anandakrishnan, R.; Aguilar, B.; Onufriev, A. V. *Nucleic Acids Res.* **2012**, *40*, W537.
(46) McPhillips, T. M.; McPhillips, S. E.; Chiu, H.-J.; Cohen, A. E.; Deacon, A. M.; Ellis, P. J.; Garman, E.; Gonzalez, A.; Sauter, N. K.; Phizackerley, R. P.; Soltis, S. M.; Kuhn, P. *J. Synchrotron Radiat.* **2002**, *9*, 401.
(47) Evans, P. *Acta Crystallogr., Sect. D: Biol. Crystallogr.* **2006**, *62*, 72.
(48) Evans, P. *Acta Crystallogr., Sect. D: Biol. Crystallogr.* **2011**, *67*, 282.
(49) Karplus, P. A.; Diederichs, K. *Science* **2012**, *336*, 1030.
(50) McCoy, A. J.; Grosse-Kunstleve, R. W.; Adams, P. D.; Winn, M. D.; Storoni, L. C.; Read, R. J. *J. Appl. Crystallogr.* **2007**, *40*, 658.
(51) Murshudov, G. N.; Skubak, P.; Lebedev, A. A.; Pannu, N. S.; Steiner, R. A.; Nicholls, R. A.; Winn, M. D.; Long, F.; Vagin, A. A. *Acta Crystallogr., Sect. D: Biol. Crystallogr.* **2011**, *67*, 355.
(52) Murshudov, G. N.; Vagin, A. A.; Dodson, E. J. *Acta Crystallogr., Sect. D: Biol. Crystallogr.* **1997**, *53*, 240.
(53) Chen, V. B.; Arendall, W. B., III; Headd, J. J.; Keedy, D. A.; Immormino, R. M.; Kapral, G. J.; Murray, L. W.; Richardson, J. S.; Richardson, D. C. *Acta Crystallogr., Sect. D: Biol. Crystallogr.* **2010**, *66*, 12.
(54) Schoner, R.; Herrmann, K. M. *J. Biol. Chem.* **1976**, *251*, 5440.
(55) Sali, A.; Blundell, T. L. *J. Mol. Biol.* **1993**, *234*, 779.
(56) Phillips, J. C.; Braun, R.; Wang, W.; Gumbart, J.; Tajkhorshid, E.; Villa, E.; Chipot, C.; Skeel, R. D.; Kale, L.; Schulten, K. *J. Comput. Chem.* **2005**, *26*, 1781.
(57) MacKerell, A. D., Jr.; Bashford, D.; Bellott, M.; Dunbrack, R. L.; Evanseck, J. D.; Field, M. J.; Fischer, S.; Gao, J.; Guo, H.; Ha, S.; Joseph-McCarthy, D.; Kuchnir, L.; Kuczera, K.; Lau, F. T.; Mattos, C.; Michnick, S.; Ngo, T.; Nguyen, D. T.; Prodhom, B.; Reiher, W. E.; Roux, B.; Schlenkrich, M.; Smith, J. C.; Stote, R.; Straub, J.; Watanabe, M.; Wiorkiewicz-Kuczera, J.; Yin, D.; Karplus, M. *J. Phys. Chem. B* **1998**, *102*, 3586.
(58) Mackerell, A. D., Jr.; Feig, M.; Brooks, C. L., 3rd *J. Comput. Chem.* **2004**, *25*, 1400.
(59) Pronk, S.; Páll, S.; Schulz, R.; Larsson, P.; Bjelkmar, P.; Apostolov, R.; Shirts, M. R.; Smith, J. C.; Kasson, P. M.; van der Spoel, D.; Hess, B.; Lindahl, E. *Bioinformatics* **2013**, *29*, 845.
(60) Glykos, N. M. *J. Comput. Chem.* **2006**, *27*, 1765.

DOI: 10.1021/jacs.5b13134
J. Am. Chem. Soc. 2016, 138, 2036−2045

(61) Humphrey, W.; Dalke, A.; Schulten, K. *J. Mol. Graphics* **1996**, *14*, 33.

DOI: 10.1021/jacs.5b13134
J. Am. Chem. Soc. 2016, 138, 2036−2045